

## Strain Sensors with Temperature Compensation Employed for Insitu Stress Monitor

Qifeng Guo<sup>1,2</sup>, Fenhua Ren<sup>\*1,2</sup>, Haoran Guo<sup>1,2</sup>, Liang Zhao<sup>1,2</sup>, Zhenxiang Yan<sup>1,2</sup>

<sup>1</sup>School of Civil and Environmental Engineering, University of Science and Technology Beijing, Beijing 100083, China

<sup>2</sup>Key Laboratory of High-Efficient Mining and Safety of Metal Mines (Ministry of Education of China), University of Science and Technology Beijing, Beijing 100083, China

\*Corresponding author, e-mail: renfh2001@sina.com

### Abstract

*The hollow inclusion strain sensors employed for in-situ stress monitor use strain gages to detect strain changes of the rock, and the detected strain changes are transmitted to resistance changes in a Wheatstone bridge, then the output voltage values of the bridge are finally used for in-situ stress calculation. In order to correct the temperature influence on the strain gages, thermistors are used to record the temperature changes during the monitor and achieve the temperature compensation. A monitor network containing 9 hollow inclusion strain sensors with temperature compensation were built to measure the in-situ stress in an undersea mine, and the measuring results discover the distribution law of 3D in-situ stress state in the mine which can be used to optimize the mining design.*

**Keywords:** hollow inclusion strain sensors, monitor network, strain gages, temperature compensation, in-situ stress

**Copyright © 2013 Universitas Ahmad Dahlan. All rights reserved.**

### 1. Introduction

Stress relief by overcoring technique and hydraulic fracturing technique are two commonly used techniques for in-situ stress monitor in the world, in which the stress relief by overcoring technique is much more suitable for in-situ stress monitor in various underground mines [1].

As a special element of information equipment, sensors are widely used in kinds of industries and engineering [2]. In mining and civil projects, sensors are also playing an important role in monitoring fields, including temperature monitor, deformation monitor, stress monitor, strain monitor, gas monitor, and water monitor [3-6]. During the monitor process, external conditions always have influence on the sensor's sensitivity and monitor results, like temperature will change the results of strain sensors during in-situ stress monitor [7-11]. Traditional temperature compensation method uses dummy gauges as compensation elements, which is not effective for sensors, such as hollow inclusion cells, which are bonded to rock during the monitor. In this paper, to solve the above problem, a full temperature compensation technique has been improved and the thermistors are used to record the temperature changes during the monitor and achieve the temperature compensation.

### 2. Strain Sensors for Stress Relief by Overcoring Technique

Stress relief of the overcore will induce deformation of the small borehole which can be detected by the monitor sensors fixed in the borehole. There are mainly 3 types of monitor sensors:

(1) Diametrical deformation gage which monitors diameter changes of the borehole during overcoring. According to the monitoring result of diameter changes at 3 directions in the same section of the borehole, the 2D stress state in a plane vertical to the borehole can be determined. To determine 3D stress state in the rock mass around the borehole, the monitor should be carried out at 3 boreholes, which are unparallel and cross at the monitor point. It is difficult and will spend high cost.

(2) Triaxial strain cell which monitors stress-relief induced strains on the borehole wall during overcoring. Usually, 12 strain values are monitored at 3 points (A, B, C) which are distributed in the same circumference with an interval of  $120^\circ$ . In one point, 4 strain values are monitored, among which  $\varepsilon_\theta$  is circumferential,  $\varepsilon_z$  is axial,  $\varepsilon_{45}$  is  $45^\circ$  inclined to the borehole axis,  $\varepsilon_{-45}$  is  $-45^\circ$  to the axis, as shown in Figure 1.

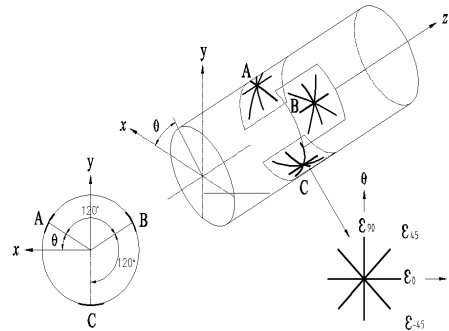


Figure.1 Sketch of Triaxial Strain Cell

Based on the following equations, from the monitored 12 strain values, 3D stress state in the rock mass around the borehole can be determined.

$$\varepsilon_\theta = \frac{1}{E} \left\{ (\sigma_x + \sigma_y) + 2(1 - \nu^2) \times \left[ (\sigma_x - \sigma_y) \cos 2\theta - 2\tau_{xy} \sin 2\theta \right] - \nu \sigma_z \right\} \quad (1)$$

$$\varepsilon_z = \frac{1}{E} [\sigma_z - \nu(\sigma_x + \sigma_y)] \quad (2)$$

$$\gamma_{\theta z} = \frac{4}{E} (1 + \nu) (\tau_{yz} \cos \theta - \tau_{zx} \sin \theta) \quad (3)$$

$$\varepsilon_{\pm 45^\circ} = \frac{1}{2} (\varepsilon_\theta + \varepsilon_z \pm \gamma_{\theta z}) \quad (4)$$

Where:  $\sigma_x$ ,  $\sigma_y$ ,  $\sigma_z$ ,  $\tau_{xy}$ ,  $\tau_{yz}$ ,  $\tau_{zx}$  are 6 components of 3D stress state at the measuring position in the OXYZ coordinate system, from which the magnitude and direction of 3 components of the principal stress, i.e.  $\sigma_1$ ,  $\sigma_2$  and  $\sigma_3$  can be determined;  $E$  and  $\nu$  are Young's modulus and Poisson's ratio of the rock mass.

It is a big progress to determine 3D stress state by measurement at one borehole.

(3) Hollow inclusion strain sensor which monitors strains on the borehole wall by strain gages embedded in a hollow inclusion wall. In triaxial strain cell technique, the strain changes on the borehole wall are detected by strain gages cemented on the borehole wall. Because the strain gages are cemented to the borehole wall in a very small area (only 1-2  $\text{cm}^2$  in a point), it is difficult to ensure cementing quality. However, the cementing quality is a key link for the strain gauge to correctly detect strain changes of the rock. To solve this problem, hollow inclusion strain cell was developed in which the strain gages are embedded in a 1.5-2 mm thick hollow cylinder wall. During making the cell, an epoxy hollow cylinder with 1 mm thick wall is firstly made; then, 12 strain gages are cemented on the outside wall of the cylinder whose arrangement are the same as in Figure 1; at last, using epoxy to pour the outside layer of the hollow cylinder wall with thickness of 0.5-1 mm. Before in-situ monitor, the whole hollow cylinder

with length of 15-20 cm is bonded to the borehole wall. As the hollow cylinder wall is very thin and flexible, the strain gages embedded in it can freely detect strains of the borehole wall as the strain gage directly bonded to rock. It not only ensures the cementing quality of the strain gages but also makes the overcore rock solidified due to injection of the cement, which is very helpful to ensure the overcoring experiment success.

Since the arrangement of the strain gages in the hollow inclusion strain sensors is all the same as in the triaxial strain cell, the calculation equations of stress from strain measured by hollow inclusion sensor are very similar to Equations (1)-(4). To modify the effect of indirect cementing to the rock of strain gages, 4 modifying factors of  $k_1$ ,  $k_2$ ,  $k_3$  and  $k_4$  are added in Equations (1)-(4) to obtain equations for calculation of stress from strain monitored by hollow inclusion strain sensor.

$$\varepsilon_{\theta} = \frac{1}{E} \left\{ \begin{array}{l} (\sigma_x + \sigma_y)k_1 + 2(1-\nu^2) \times \\ \left[ (\sigma_y - \sigma_x) \cos 2\theta - \right. \\ \left. 2\tau_{xy} \sin 2\theta \right] k_2 - \nu\sigma_z k_4 \end{array} \right\} \quad (5)$$

$$\varepsilon_z = \frac{1}{E} [\sigma_z - \nu(\sigma_x + \sigma_y)] \quad (6)$$

$$\gamma_{\theta z} = \frac{4}{E} (1 + \nu) (\tau_{yz} \cos \theta - \tau_{zx} \sin \theta) k_3 \cdot \quad (7)$$

The values of  $k_1$ ,  $k_2$ ,  $k_3$  and  $k_4$  are related to the values of radius of the small borehole, internal radius of the hollow inclusion, shear modulus and Poisson's ratio of the rock and hollow inclusion. So they should be particularly calculated for each monitor.

### 3. Full Temperature Compensation Technique

The hollow inclusion strain sensor and triaxial strain sensor both use strain gages to detect strain changes of the rock. The detected strain changes are transmitted to resistance changes in a Wheatstone bridge and the output voltage values of the bridge are finally used for stress calculation. Because the strain gages are susceptible to temperature changes, correct temperature compensation is critical for reliability and accuracy of calculated results of the monitor. Traditional temperature compensation method uses dummy gauges as compensation elements, which is not effective for devices, such as hollow inclusion sensor, which are bonded to rock during the measurement. To solve this problem, a full temperature compensation technique has been improved and the thermistors are used to record the temperature changes during the monitor and achieve the temperature compensation, based on which following steps have been added to the procedure of in-situ stress monitor with strain gages as the detecting elements.

(1) Resistance elements in the Wheatstone bridge are all of low temperature coefficient except the strain gauge from the in-situ monitor sensor, which ensures no considerable additional voltage output produced due to temperature change.

(2) Temperature changes at the monitor point are continuously recorded by a thermistor during overcoring.

(3) After completion of the overcoring test, the overcore with the monitor sensors inside is calibrated in a temperature controllable oven to get thermal strain rate, i.e. strain value induced by temperature change of  $1^{\circ}\text{C}$ , for each strain gauge.

From the calibrated thermal strain rate and recorded temperature change during overcoring, the additional thermal strain values for every strain gauge can be determined and then eliminated from the total monitored strain values to get the correct strain values actually caused by stress relief.

#### 4. Installation of Hollow Inclusion Strain Sensors

The Measuring principle and process of in-situ stress monitor with stress relief by overcoring technique consist of following 4 steps, as shown in Figure 2:

(1) Drill a big borehole with diameter of 130mm from the surface of tunnels, roadways or shafts into the rock mass to access the monitor point. The length of the borehole is about 3 times of the diameter (width) of the tunnels, roadways or shafts to ensure stress state at the measuring point is original, i.e. undisturbed by excavation.

(2) Drill a small borehole with diameter of 37mm and length of 40-50mm from the end of big borehole. The small borehole is concentric with the big borehole and used for installation of the hollow inclusion strain sensor.

(3) Fix the monitor device at the central section of the small borehole.

(4) Extend the big borehole using a thin-walled drill with outside diameter of 130mm. Along with extension of the big borehole, the cylindrical rock core, which is called overcore, is gradually stress released. Deformation of small borehole caused by stress relief during overcoring is detected by the measuring device fixed at the centre of the small borehole. When the value of the deformation is stabilized, the overcoring drilling is stopped. From the recorded deformation of the small borehole during overcoring, the stress state around the borehole can be determined according to known equations.

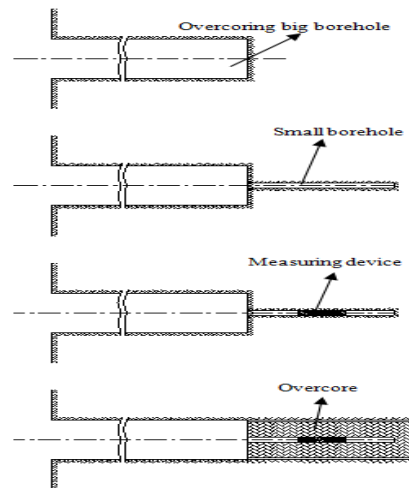


Figure 2. Monitor Steps of Stress Relief by Overcoring Technique

#### 5. Engineering Application in an Undersea Mine

##### 5.1. Actual Layout of the Monitor Network

Based on the above principles, meticulously selected 9 measuring points formed the monitor network, whose conditions are shown in Table 1. In the Table, "burring depth" is the vertical distance of monitor position to the ground surface; "borehole" is drilled from the side wall of roadways to access the measuring point; RQD is calculated from the drilled cores of the borehole, which reflects integrity of the rock mass in the monitor point.

Table 1. Layout of Monitor Network with Relevant Conditions

No.	Burring depth/m	Length of borehole/m	RQD/%
1	512	8.10	48.5
2	512.5	9.44	64.2
3	647	9.13	47.4
4	602.2	9.71	61.3
5	603	9.64	88.4
6	693	10.79	75.3
7	693	9.20	82.7
8	750	8.51	66.5
9	553	8.63	81.2

## 5.2. Results of Stress relief by Overcoring Experiments

During overcoring, the strain value induced by stress relief at the beginning was very small and some strain gages even detected minus strain values which could be attributed to "excavation effect" of the overcoring. Along with increase of the overcoring distance, the strain values were gradually increased and sharp strain changes appeared as the overcoring close to the section where the strain gages bonded. After the overcoring passed the section, the strain values were gradually stabilized. The finally stabilized strain values detected by every strain gages of the monitor network are shown in Table 2, which are original data for in-situ stress monitor.

Table 2. Results of Stress Relief by Overcoring Experiments

Monitor Points	Finally stabilized stain values during overcoring / $\mu\epsilon$											
	A				B				C			
	$\epsilon_z$	$\epsilon_{45}$	$\epsilon_{\theta}$	$\epsilon_{-45}$	$\epsilon_z$	$\epsilon_{45}$	$\epsilon_{\theta}$	$\epsilon_{-45}$	$\epsilon_z$	$\epsilon_{45}$	$\epsilon_{\theta}$	$\epsilon_{-45}$
1	280	587	407	343	233	858	58	962	263	771	919	77
2	426	598	342	465	426	986	156	1010	397	860	908	166
3	319	1006	1214	-	319	759	240	767	303	694	91	892
4	442	603	80	850	513	841	735	375	379	658	555	397
5	206	1399	1036	498	202	1025	308	984	197	551	402	357
6	240	516	635	129	255	1047	-186	1460	251	763	984	-96
7	200	846	929	142	189	860	226	764	195	783	380	631
8	345	1055	1099	240	282	1017	701	660	300	1021	182	1117
9	243	438	394	258	232	662	703	235	226	450	63	652

## 5.3. Temperature Compensation Results

Based on the operation rules of full temperature compensation technique, as introduced in Section 2.3, the temperature calibration experiments were completed. The experimental results are shown in Table 3.

Table 3. Temperature Compensation Results

Monitor points	Strain value per 1°C of temperature change / $\mu\epsilon$											
	A				B				C			
	$\epsilon_z$	$\epsilon_{45}$	$\epsilon_{\theta}$	$\epsilon_{-45}$	$\epsilon_z$	$\epsilon_{45}$	$\epsilon_{\theta}$	$\epsilon_{-45}$	$\epsilon_z$	$\epsilon_{45}$	$\epsilon_{\theta}$	$\epsilon_{-45}$
1	64	40	13	15	21	32	13	40	60	35	12	40
2	42	24	5	19	43	26	4	24	39	10	2	14
3	34	20	4	16	35	21	3	20	32	8	2	11
4	35	25	5	32	50	31	10	24	20	30	5	30
5	17	20	15	17	18	17	29	33	16	15	18	21
6	31	-27	1	5	50	-42	-9	12	37	32	-8	0
7	22	45	17	38	16	31	29	0	18	30	21	23
8	37	73	56	54	17	53	40	36	22	59	36	34
9	20	52	5	37	27	39	24	32	22	33	315	13

## 5.4. The Values of E, $\nu$ and k Factors Obtained with Biaxial Loading Tests

Equation (5)-(7) show that to calculate stress state from the measured strain, the values of  $E$ ,  $\nu$ ,  $k_1$ ,  $k_2$ ,  $k_3$  and  $k_4$  are needed.

The values of  $E$  and  $\nu$  are determined through biaxial loading test. After completion of the overcoring experiment, the hollow inclusion strain sensor is still in the overcore which can be used to monitor strain value caused by biaxial loading exerted to the overcore. The values of  $E$  and  $\nu$  can be calculated from the strain values caused by biaxial loading based on Equations

(8) and (9). The values of  $E$  and  $\nu$  obtained from biaxial test are mechanical parameters of rock really at the monitor point.

$$E = k_1 \frac{P_0}{\varepsilon_\theta} \frac{R^2}{(R^2 - r^2)} \quad (8)$$

$$\nu = \frac{\varepsilon_\theta}{\varepsilon_z} \quad (9)$$

Where:  $P_0$  is biaxial load;  $\varepsilon_\theta$ ,  $\varepsilon_z$  are averaged circumferential and axial strain caused by biaxial load;  $R$ ,  $r$  are external and internal radius of the overcore.

The calculated values of  $E$  and  $\nu$  and relevant values of  $k_1$ ,  $k_2$ ,  $k_3$ ,  $k_4$  are shown in Table 4.

Table 4. Values of  $E$ ,  $\nu$ ,  $k_1$ ,  $k_2$ ,  $k_3$ ,  $k_4$  at 9 Monitor Points

Monitor Points	$E$ /GPa	$\nu$	$k_1$	$k_2$	$k_3$	$k_4$
1	50	0.25	1.045	1.061	1.030	0.978
2	52	0.22	1.120	1.138	1.076	0.917
3	55	0.20	1.122	1.140	1.077	0.894
4	60	0.21	1.141	1.157	1.088	0.891
5	55	0.25	1.155	1.166	1.098	0.924
6	50	0.36	1.132	1.556	1.087	1.000
7	56	0.28	1.139	1.158	1.089	0.956
8	51	0.35	1.148	1.159	1.091	0.824
9	56	0.28	1.139	1.158	1.089	0.956

## 5.5. Distribution Law of the 3D In-situ Stress State

Table 5. Monitor Results of 3D In-situ Stress State

Monitor points	$\sigma_1$			$\sigma_2$			$\sigma_3$		
	Magnitude /MPa	Bearing /( $^\circ$ )	Dip /( $^\circ$ )	Magnitude /MPa	Bearing /( $^\circ$ )	Dip /( $^\circ$ )	Magnitude /MPa	Bearing /( $^\circ$ )	Dip /( $^\circ$ )
1	24.55	129	4	16.35	-138	2	14.49	133	-85
2	24.64	-111	3	15.68	155	82	15.02	161	-10
3	29.57	112	-3	19.56	-177	-80	15.48	-156	-9
4	28.88	103	1	16.54	10	76	14.77	13	-8
5	30.17	110	-16	18.83	24	-11	16.94	236	-70
6	31.50	-80	2	19.08	230	-79	17.54	10	-10
7	29.77	-83	4	20.84	-8	-74	19.63	8	15
8	33.22	119	-10	19.93	-89	-82	17.10	208	-8
9	25.71	-45	-13	14.00	14	73	13.00	50	-20

From the temperature calibration results as listed in Table 3 and the recorded temperature change at every measuring point during overcoring as given in Table 2, the additional strain values caused by temperature changes can be determined. Subtracting the additional strain values from the recorded finally stabilized strain values as shown in Table 2, the strain values actually induced by stress relief are obtained. With these strain values and based on Equations (4)-(7), the 3D stress state at every monitor point is determined. The 3D principal stress state is shown in Table 5. In the table,  $\sigma_1$ ,  $\sigma_2$ , and  $\sigma_3$  are major, intermediate and minor principal stresses in the monitor point respectively.

The preliminary works have achieved the in-situ stress as shown in Table 6.

Table 6. Preliminary Monitor Results of 3D In-situ Stress State

Monitor points	Depth / m	$\sigma_1$			$\sigma_2$			$\sigma_3$		
		Magnitude / MPa	Bearing / (°)	Dip / (°)	Magnitude / MPa	Bearing / (°)	Dip / (°)	Magnitude / MPa	Bearing / (°)	Dip / (°)
1	75	6.01	288.5	-6.3	3.81	198.0	-4.9	2.56	250.4	82.0
2	420	19.27	284.1	-21.3	11.05	18.5	-11.1	10.88	134.4	-65.7
3	420	19.39	120.4	-14.9	10.92	169.2	68.1	9.44	34.7	15.8
4	150	7.73	280.9	-5.2	5.48	9.4	16.6	4.50	27.7	72.5

The values of maximum horizontal principal stress ( $\sigma_{h,max}$ ), minimum horizontal principal stress ( $\sigma_{h,min}$ ) and vertical principal stress ( $\sigma_v$ ) are all increased with depth and show approximately linear increasing regularity. Using linear regression method, the relations of magnitude of the stresses and the burring depth  $H$  are expressed as follows:

$$\sigma_{h,max} = 1.433 + 0.043H$$

$$\sigma_{h,min} = 1.304 + 0.024H$$

$$\sigma_v = 0.07 + 0.028H$$

## 6. Conclusion

(1) Hollow inclusion strain sensor for stress relief by overcoring technique is much suitable for in-situ stress monitor in underground mines due to its remarkable advantages: convenient to access the measuring points which will greatly save the measuring cost; to determine 3D *in-situ* stress state in a measuring point by only one borehole's measurement, which will highly increase the measuring efficiency.

(2) The full temperature compensation technique using thermistors to record the temperature changes during the monitor is very effective for reducing the temperature influence and monitor error during the in-situ stress monitor.

(3) The in-situ stress distribution law achieved through improved strain sensors with temperature compensation is very dependable, and it provides basis for optimum design of the mine in following aspects: overall layout of the mining engineering, selection of the optimal shape of underground roadways and stopes, selection of most suitable mining method and steps, design of reliable support and reinforcement of mining structures, prediction of rock burst, mining seismicity and other dynamic disasters.

## Acknowledgement

This work was supported by the National Natural Science Foundation of China (No. 51034001 & No.11002021).

## References

- [1] Meifeng Cai, Hua Peng. Advance of in-situ stress measurement in China. *Journal of Rock Mechanics and Geotechnical Engineering*. 2011; 3(4): 373-384.
- [2] Zhuping Wang, Shunan Zhong, Dandan Nie, Ruqing Liu. Mathematical modeling of micro thermal shear stress sensor. *Beijing Ligong Daxue Xuebao*. 2010; 30(9): 1112-1116.
- [3] Kärki Satu, Lekkala Jukka, Kuokkanen Hannu, Halttunen Jouko. Development of a piezoelectric polymer film sensor for plantar normal and shear stress measurements. *Sensors and Actuators, A: Physical*. 2009; 154(1): 57-64.
- [4] J Parthenios, DG Katerelos, GC Psarras, C Galiotis. Aramid fibers: a multifunctional sensor for monitoring stress/strain fields and damage development in composite materials. *Engineering Fracture Mechanics*. 2002; 69(9): 1067-1087.
- [5] Villatoro Joel, Minkovich Vladimir P, Monzón-Hernández, David. Temperature-independent strain sensor made form tapered holey optical fiber. *Optics Letters*. 2006; 31(3): 305-307.

- [6] Jun Huang, Zude Zhou, Xiaoyan Wen, Dongsheng Zhang. A diaphragm-type fiber Bragg grating pressure sensor with temperature compensation. *Measurement: Journal of the International Measurement Confederation*. 2013; 46(3): 1041-1046.
- [7] Brunelli D, Balsamo D, Paci G, Benini L. Temperature compensated time synchronisation in wireless sensor networks. *Electronics Letters*. 2012; 48(16): 1026-1028.
- [8] Pramanik C, Islam T, Saha H. Temperature compensation of piezoresistive micro-machined porous silicon pressure sensor by ANN. *Microelectronics Reliability*. 2006; 46(2-4): 343-351.
- [9] Ke Pang, Shengcai Zhang, Spying Yao, Wei Zhang. On-chip temperature compensation technology of high-temperature polysilicon pressure sensor. *Chinese Journal of Sensors and Actuators*. 2004; 17(1): 118-121.
- [10] Amador R, Polanco A, Hernandez H, Gonzalez E, Nagy A. Technological compensation circuit for accurate temperature sensor. *Sensors and Actuators, A: Physical*. 1998; 69(2): 172-177.
- [11] Kovács Klára, Hussami Linda L, Rábai, Gyula. Temperature compensation in the oscillatory bray reaction, Sensors and Actuators. *Journal of Physical Chemistry A*. 2005; 109(45): 10302-10306.
- [12] Hongpu Kang, Jian Lin, Xiao Zhang. Research and application of in-situ stress measurement in deep mines. *Chinese Journal of Rock Mechanics and Engineering*. 2007; 26(5): 929-933.